Bulletin of the Seismological Society of America, Vol. 88, No. 6, pp. 1392–1401, December 1998

Stochastic Finite-Fault Modeling of Ground Motions from the 1994 Northridge, California, Earthquake. I. Validation on Rock Sites

by Igor A. Beresnev and Gail M. Atkinson

Abstract The stochastic method of simulating ground motions from finite faults is validated against strong-motion data from the M 6.7 1994 Northridge, California, earthquake. The finite-fault plane is subdivided into elements, each element is assigned a stochastic ω^2 spectrum, and the delayed contributions from all subfaults are summed in the time domain. Simulated horizontal acceleration time histories and Fourier spectra at 28 rock sites are compared with observations. We first perform simulations using the slip distribution on the causative fault derived from strong-motion, teleseismic, GPS, and leveling data (Wald *et al.,* 1996). We then test the performance of the method using quasi-random distributions of slip and alternative hypocenter locations; this is important because the rupture initiation point and slip distribution are in general not known for future earthquakes.

The model bias is calculated as the ratio of the simulated to the observed spectrum in the frequency band of 0.1 to 12.5 Hz, averaged over a suite of rock sites. The mean bias is within the 95% confidence limits of unity, showing that the model provides an accurate prediction of the spectral content of ground motions on average. The maximum excursion of the model bias from the unity value, when averaged over all 28 rock stations, is a factor of approximately 1.6; at most frequencies, it is below a factor of 1.4.

Interestingly, the spectral bias and the standard deviation of the stochastic simulations do not depend on whether the fault slip distribution and hypocenter location are based on data or are randomly generated. This suggests that these parameters do not affect the accuracy of predicting the average characteristics of ground motion, or they may have their predominant effect in the frequency range below about 0.1 Hz (below the range of this study). The implication is that deterministic slip models are not necessary to produce reasonably accurate simulations of the spectral content of strong ground motions. This is fortunate, because such models are not available for forecasting motions from future earthquakes. However, the directivity effects controlled by the hypocenter location are important in determining peak ground acceleration at individual sites.

Although the method is unbiased when averaged over all rock sites, the simulations at individual sites can have significant errors (generally a factor of 2 to 3), which are also frequency dependent. Factors such as local geology, site topography, or basin-propagation effects can profoundly affect the recordings at individual stations. To generate more accurate site-specific predictions, empirical responses at each site could be established.

Introduction

Stochastic modeling of earthquake radiation is widely used in the prediction of strong ground motions (Hanks and McGuire, 1981; Boore, 1983, 1986, 1996; Boore and Atkinson, 1987; Chin and Aki, 1991; Atkinson and Boore, 1997; Toro *et al.,* 1997; Atkinson and Beresnev, 1998). The method assumes that high-frequency earthquake motions can be represented as band-limited Gaussian noise having an ω^2 mean spectrum. A limitation of the model, as it is

most commonly employed, is that earthquakes are treated as point sources. There is growing recognition that finite-fault effects, including rupture geometry and directivity, can profoundly influence the character of strong-ground motions, in both the near- and far-field regions (Hartzell, 1978; Irikura, 1983; Joyner and Boore, 1986; Heaton and Hartzell, 1989; Somerville *et al.,* 1991; Hutchings, 1994; Tumarkin and Archuleta, 1994; Tumarkin *et al.,* 1994; Zeng *et al.,* 1994; Atkinson and Silva, 1997). To accommodate these effects, Silva *et al.* (1990), Schneider *et al.* (1993), and Beresnev and Atkinson (1997) extended the stochastic modeling technique to consider rupture along a finite-fault plane. The stochastic finite-fault model has been validated against the *M* 6.9 1989 Loma Prieta, California (Schneider *et al.,* 1993), the *M* 8.0 1985 Michoacan, Mexico, the *M* 8.0 1985 Valparaiso, Chile, and the *M* 5.8 1988 Saguenay, Québec, events (Beresnev and Atkinson, 1997).

The purpose of this study is to validate the stochastic finite-fault simulation technique against multiple free-field hard-rock stations that recorded strong motions from the *M* 6.7 1994 Northridge, California, mainshock (Chang *et al.,* 1996, Table 1). The restriction to rock sites eliminates complications introduced by pronounced site response and nonlinearity; these effects are discussed in a companion article (Beresnev *et al.,* 1998). The database for the validation exercise includes all rock records contained in the Southern California Earthquake Center (SCEC) strong-motion database (Tumarkin *et al.,* 1996; Wald, 1997; also http://smdb.crustal.ucsb.edu/). Records that can be categorized as rock are determined following the classification of Chang *et al.* (1996) or the information on site geology provided by the SCEC database; there are 28 rock stations identified on this basis.

Stochastic Finite-Fault Simulation Method

The simulation method is presented by Beresnev and Atkinson (1997, 1998). All simulations are performed using the FORTRAN code FINSIM (Beresnev and Atkinson, 1998). The method uses a traditional kinematic finite-source model (Hartzell, 1978), in which the rupture initiates at the hypocenter and propagates radially from it. The velocity of rupture propagation is assumed to equal 0.8 times the shear-wave velocity. A rectangular fault is assumed. The fault plane is subdivided into rectangular elements (subfaults); each subfault is triggered as the rupture reaches its center. The subfault acceleration time history is propagated to the observation point using empirical distance-dependent duration, geometric attenuation, and attenuation (Q) models (Boore and Atkinson, 1987; Beresnev and Atkinson, 1997). The user-defined character of the empirical operators makes the method readily applicable to any particular region of interest.

The method of Boore (1983, 1996) is used to generate stochastic acceleration time histories from each of the subfaults. The ω^2 spectrum of the subfault (Boore, 1983) is multiplied by the normalized spectrum of a limited-duration Gaussian noise sample. This produces a subfault spectrum that has a stochastic character. The corner frequency of the underlying point-source ω^2 spectrum (f_0) and the corresponding subfault moment (m_0) are derived from the subfault size (Δl):

$$f_0 = (yz/\pi)\beta/\Delta l, \tag{1}$$

$$m_0 = \Delta\sigma\ \Delta l^3, \tag{2}$$

where $\Delta\sigma$ is the Kanamori–Anderson (1975) "stress parameter" (fixed at 50 bars), β is the shear-wave velocity, y is the ratio of rupture velocity to β (fixed at 0.8), and z is the parameter defining the strength of high-frequency radiation (Beresnev and Atkinson, 1997, equations 14 and 16, respectively). The number of subfault triggerings is adjusted to conserve the total moment of the modeled earthquake. Inhomogenuous slip distribution on the target fault is allowed.

In the initial formulation of the method, the parameter z in equation (1) was a constant, whose value could be obtained by calibration against empirical data. In a subsequent refinement, we have linked z to the maximum velocity of slip on the fault, in order to give this parameter a clear physical meaning. The maximum slip velocity on a dislocation that radiates an ω^2 spectrum is derived from equation (8) of Beresnev and Atkinson (1997): $v_m = U/e\tau$, where U is the final displacement, e is the base of natural logarithm, and $\tau \equiv 1/2\pi f_0$. Using equation (1) and the definition of stress parameter $\Delta\sigma \equiv \mu(U/\Delta l)$, where μ is the shear modulus, we obtain

$$v_m = (2yz/e)\ (\Delta\sigma/\rho\beta), \tag{3}$$

where ρ is density. Thus, the parameter z directly controls the maximum slip velocity on the fault. It follows from shear-dislocation theory that z has a value of 1.68, using the standard convention for the definition of dislocation rise time (Beresnev and Atkinson, 1997, p. 70). A value of $z > 1.68$ implies a "faster" slip, while $z < 1.68$ implies slower slip. The ratio of a particular z value to 1.68 can be considered as a high-frequency radiation-strength factor (s), because a high value of z will enhance the acceleration spectral amplitudes at high frequencies (above f_0), whereas a low z value will have the opposite effect.

Our modeling of the *M* 8.0 1985 Michoacan and Valparaiso subduction-zone events accurately reproduced strong ground motions using $s = 1.0$. We anticipate that the natural variability of slip velocities on faults will lead to radiation-strength factors generally departing from unity. Since the level of high-frequency radiation is proportional to f_0^2 (Boore, 1983, equation 3; Atkinson and Beresnev, 1997), spectral amplitudes at high frequencies vary as z^2. Thus, an increase in the s factor from, say, 1 to 2, would increase high-frequency spectral amplitudes by a factor of 4. For this reason, we would generally not expect s to vary

from its standard value of unity by more than about a factor of 2. For example, $s = 1.6$ is the derived value from the 28 rock sites that recorded the Northridge mainshock (see later).

Simulation Parameters

The locations of the 28 rock stations used in the validation are shown in Figure 1; their geography is summarized in Table 1. Station names are those adopted in the SCEC database. A summary of simulation parameters is given in Table 2.

The moment, slip distribution, and fault geometry are adopted from the preferred model of Wald *et al.* (1996, Fig. 4d and Table 5). Wald *et al.*'s (1996) slip distribution is reproduced in Figure 2a. The overall rupture dimensions are 18 by 24 km, while the effective area of slip, shown in Figure 2a, is 14 by 21 km. We discretize the fault into 5- by 5-km elements and derive the individual slips based on contours. Note that each subfault can only trigger an integer number of times. Because their moments then become discrete and can only be multiples of m_0 in equation (2) (Beresnev and Atkinson, 1997, p. 72), adjustments were made in individual slips to match the target moment. The resulting discretized model is shown in Figure 2b, where the entire fault plane is shown. The uppermost and lowermost rows of subfaults in this model have zero slip, although all subfaults will radiate in the random slip models considered below.

We emphasize that the approximate subfault size should be considered an internal parameter of the finite-fault models and cannot be arbitrarily chosen on a case-by-case basis. The total radiation has a square-root dependence on the subfault size; thus model calibration, including determination of appropriate Δl, is essential (Beresnev and Atkinson, 1998, equation 6). A semi-empirical rule, based on a number of validation studies, establishes that the subfaults be approximately equivalent to M 5 to 6.5 earthquakes, depending upon the size of target event (Silva *et al.*, 1990; Schneider *et al.*, 1993; Beresnev and Atkinson, 1998). This rule has some theoretical justification. In general, the subfault corner frequency should be below the frequency range of simulation, imposing a minimum size Δl, and thus a minimum magnitude for the subevent. This constraint reduces the model dependence on subfault size. On the other hand, the maximum Δl is also limited, because a sufficient number of subevents is needed to produce realistic-looking accelerograms (Beresnev and Atkinson, 1998, pp. 28–29). Based on

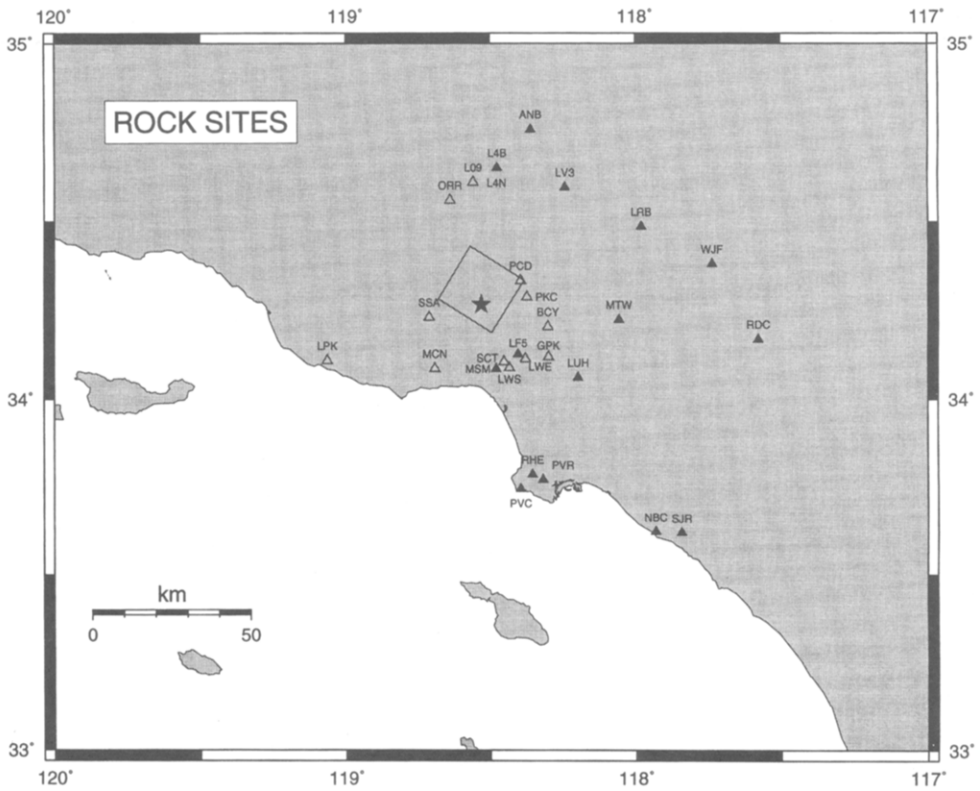

Figure 1. The rock sites used in the simulations (triangles). Open triangles mark the stations surrounding the fault plane at different azimuths, whose trace-by-trace simulations are presented in Figure 3. The surface projection of the mainshock rupture is outlined by the box (Wald *et al.*, 1996). The fault plane dips to the southwest at 40°, with the top edge at a depth of 5 km and the bottom edge at a depth of 21.1 km. The epicenter is marked with the star.

Table 1
Rock Stations

Station Name	Latitude	Longitude	Location	Hypocentral Distance (km)	Agency*
ANB	34.758	−118.361	Antelope Buttes	66.1	CDMG
BCY	34.204	−118.302	USC #59	29.1	USC
GPK	34.120	−118.300	Los Angeles–Griffith Observatory	30.9	USGS
L09	34.610	−118.560	Lake Hughes #9	48.5	CDMG
L4B	34.650	−118.477	Lake Hughes #4B	53.0	CDMG
L4N	34.650	−118.478	Lake Hughes #4	53.0	CDMG
LF5	34.127	−118.405	USC #14	24.5	USC
LPK	34.109	−119.065	Point Mugu–Laguna Park	53.1	CDMG
LRB	34.486	−117.980	Littlerock–Brainard Canyon	63.0	CDMG
LUH	34.062	−118.198	Los Angeles–University Hospital Grounds	40.3	CDMG
LV3	34.596	−118.243	Leona Valley #3	54.5	CDMG
LWE	34.114	−118.380	USC #17	26.3	USC
LWS	34.089	−118.435	USC #16	25.2	USC
MCN	34.087	−118.693	Malibu Canyon–Monte Nido Fire Station	27.2	USGS
MSM	34.086	−118.481	USC #15	24.1	USC
MTW	34.224	−118.057	Mt. Wilson–Caltech Seismic Station	48.5	CDMG
NBC	33.623	−117.931	Newport Beach–Newport Blvd & Coast Hwy	88.3	CDMG
ORR	34.560	−118.640	Castaic–Old Ridge Route	44.4	CDMG
PCD	34.334	−118.396	Pacoima Dam Downstream	27.1	CDMG
PKC	34.288	−118.375	Pacoima–Kagel Canyon	25.9	CDMG
PVC	33.746	−118.396	Rancho Palos Verdes–Hawthorne Blvd	56.5	CDMG
PVR	33.772	−118.319	Palos Verdes Reservoir Abutment Bldg	56.1	USGS
RDC	34.169	−117.579	Rancho Cucamonga–Deer Canyon	90.7	CDMG
RHE	33.787	−118.356	Rolling Hills Estates–Rancho Vista School	53.5	CDMG
SCT	34.106	−118.454	Stone Canyon Reservoir Dam	23.6	SCEC
SJR	33.620	−117.842	San Joaquin Reservoir Left Abutment	94.0	USGS
SSA	34.231	−118.713	Santa Susana	24.9	DOE
WJF	34.381	−117.737	Wrightwood–Jackson Flat	78.7	CDMG

*Name of agency that collected the data. CDMG: California Division of Mines and Geology; DOE: Department of Energy; SCEC: Southern California Earthquake Center; USC: University of Southern California; USGS: United States Geological Survey.

Table 2
Modeling Parameters

Parameter	Parameter Value
Fault orientation	strike 122°, dip 40°
Fault dimensions along strike and dip (km)	20 by 25
Fault depth range (km)	5–21.1
Mainshock moment (dyne-cm)	1.3×10^{26}
Subfault dimensions (km)	5 by 5
Stress parameter (bars)	50
Radiation-strength factor	1.6
Number of subsources summed	17
$Q(f)$	$150f^{0.5}$
Geometric spreading	$1/R$
Windowing function	Saragoni–Hart
Kappa	0.05
Local amplification	Boore–Joyner (1997) western North America generic rock site
Crustal shear-wave velocity (km/s)	3.7
Rupture velocity	0.8 × (shear-wave velocity)
Crustal density (g/cm^3)	2.8

these constraints, FINSIM establishes a convention by which the subfault size varies between approximately 5 and 15 km, which are considered well-calibrated values. The existence of a lower limit implies that the finite-fault methodology is applicable to seismic events with magnitudes exceeding approximately 5.5, while smaller events can be considered point sources (Beresnev and Atkinson, 1998, p. 29). This conclusion is consistent with modeling results for the empirical California database (Atkinson and Silva, 1997).

For the hypocentral-distance range of the observations, ranging from 24 to 94 km, a geometric spreading operator of $1/R$ was applied. The duration of motion is assumed to equal the source duration. The adopted form of the regional quality factor, $Q = 150\sqrt{f}$, is characteristic of southern California (Hartzell *et al.*, 1996). All simulated spectra were amplified by the crustal response of a generic western North American rock site (Boore and Joyner, 1997, Table 3) and attenuated by the kappa operator with $\kappa = 0.05$ (Anderson and Hough, 1984), which is the generic California value for events of this magnitude (Atkinson and Silva, 1997).

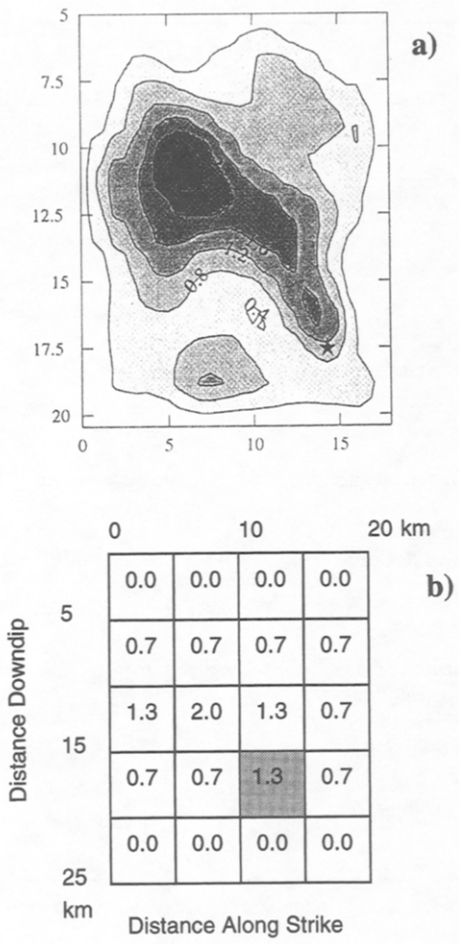

Figure 2. (a) Effective area (14 by 21 km) of Northridge mainshock rupture. The hypocenter is marked with the star. The contours indicate slip in meters. The full fault dimensions are 18 and 24 km along strike and dip, respectively (after Wald *et al.*, 1996). (b) Finite-fault model used in simulations. The subfaults are 5 by 5 km. The slip on individual subfaults is derived from contours and changes discretely in steps of m_0. The hypocenter is at the center of the subfault shown in dark color. The full fault dimensions are shown.

We determined, by trial-and-error, that the value of radiation-strength factor that best fits the recorded spectra (0.1 to 12.5 Hz) is $s = 1.6$. This is the only parameter, other than the slip distribution, that is fine-tuned or specific to this simulation exercise.

Data

The results of finite-fault simulations are validated against recorded horizontal acceleration time histories and their Fourier amplitude spectra. The recorded accelerograms, obtained through the SCEC strong-motion database, do not all have the same sampling rate. Recorded traces with sampling intervals less than 0.01 sec were low-pass filtered and decimated to 0.01 sec. Other records were originally sampled at 0.01 or 0.02 sec. Each simulated trace has the same sampling interval as the recorded trace to which it is compared. A 12-sec window of the observed shear wave was used to calculate the Fourier spectrum. The spectra of the two observed horizontal components were geometrically averaged.

Results

Observations and Simulations at Individual Stations and Estimation of Model Bias

We first choose a subset of 12 stations near the surface projection of the fault, surrounding it at various azimuths (open triangles in Fig. 1). The distribution of these stations provides a reasonable coverage of the directivity effects from the mainshock rupture. Figure 3 compares the recorded and simulated accelerograms and Fourier spectra at these 12 stations, arranged clockwise from station PCD, which is located approximately updip from the fault. The 12-sec windows of the two observed horizontal components are shown below the spectra, except for station SSA, where only one recorded component is available. The stochastic simulation program, with parameters given earlier, was used to generate a random horizontal component, which is shown as the bottom trace below the spectra. The fault slip distribution derived from the preferred model of Wald *et al.* (1996) is used.

Model bias is commonly defined as the ratio of simulated to observed Fourier spectrum, averaged over all stations (Abrahamson *et al.*, 1990; Schneider *et al.*, 1993; Atkinson and Boore, 1998). The frequency range of this study is 0.1 to 12.5 Hz. Note that the bias estimated in this way is insensitive to whether acceleration or velocity time histories are used, because they have identical model bias as computed in the frequency domain (treating bias in the frequency domain is also useful for engineering applications). Figures 4 and 5 present the model bias calculated on the basis of 12 close-in stations, representing the directivity effects on the spectra (Fig. 3), and all 28 rock sites, respectively. The hatched bands indicate the 95% confidence limits of the mean, calculated from the t distribution, and the dashed lines show ± 1 standard deviation. The standard deviation provides a measure of prediction uncertainty for individual stations, while the confidence band on the mean provides a measure of the uncertainty on the mean bias of the model.

We base our simulations for each site on a single stochastic realization of the acceleration spectrum, rather than an average value over many realizations. This is justified, because the stochastic variability is small in relation to natural variability in source processes, and our primary interest is in the mean bias taken over many stations.

Figure 3 shows that the duration of strong ground motion and the shape and the amplitude of the Fourier spectrum

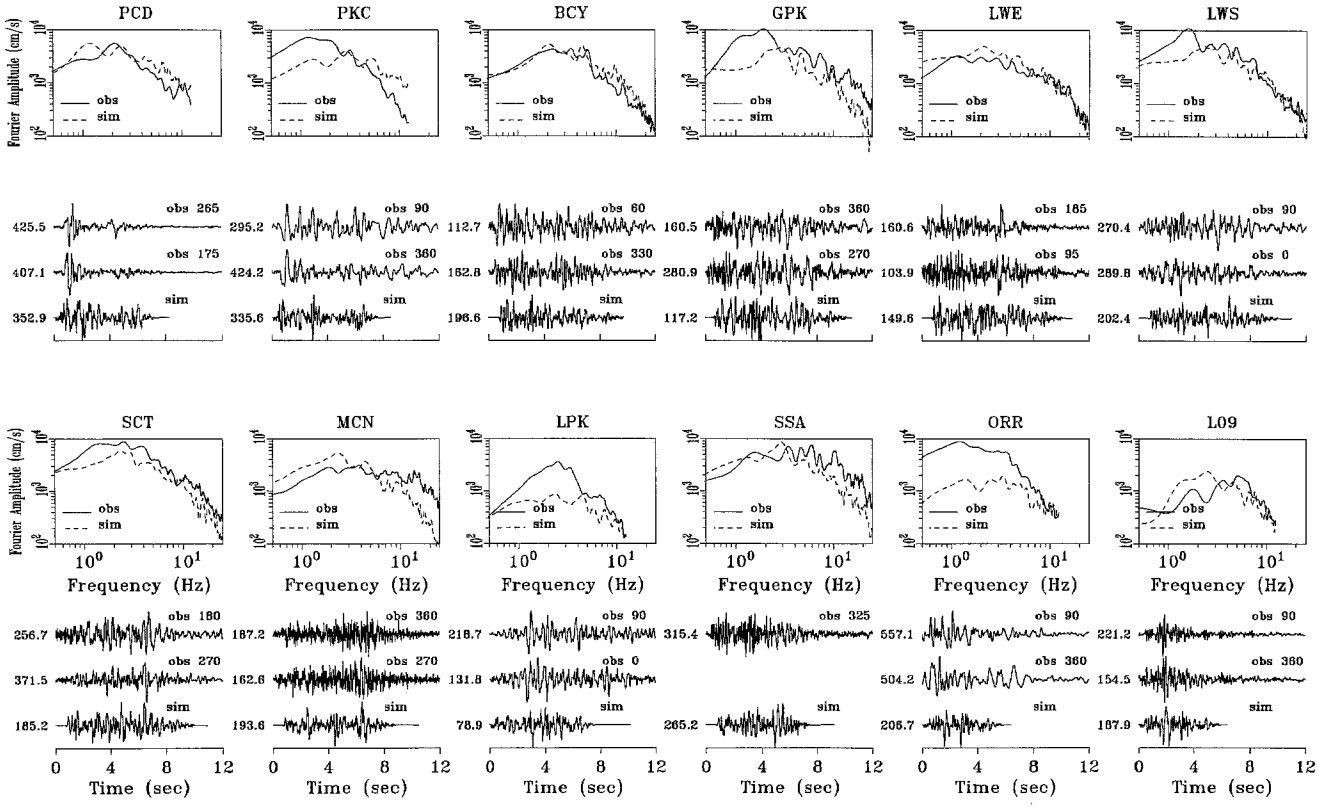

Figure 3. Recorded and simulated accelerograms and Fourier spectra at 12 stations surrounding the fault plane. The stations are shown as open triangles in Figure 1. The sites are arranged clockwise from station PCD. The observed and simulated spectra are shown by the solid and dashed lines, respectively. The two upper traces below the spectra are the observed horizontal accelerations, with azimuth of the component indicated above each trace. The peak ground acceleration in cm/sec^2 is shown to the left of the traces.

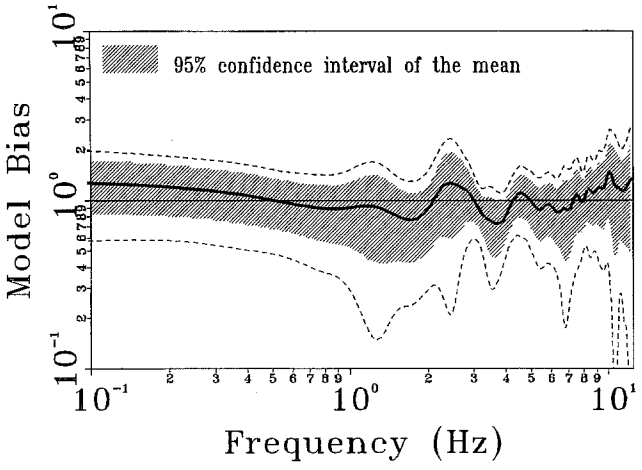

Figure 4. Model bias showing the ratio of simulated to observed spectrum, averaged over 12 close-in stations shown as open triangles in Figure 1. The observed spectrum at each site is calculated as the geometric average of the spectra of two horizontal components. Dashed line shows ± 1 standard deviation.

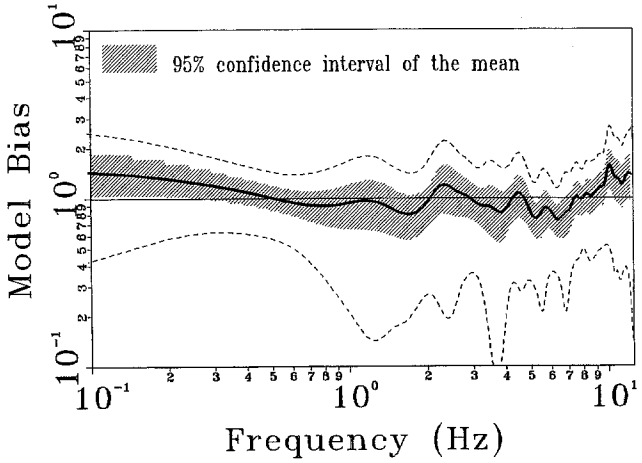

Figure 5. Model bias and standard deviation for all 28 rock stations.

are generally well matched by the stochastic simulations, although significant discrepancies exist at certain sites. The model gives an accurate prediction on average: The mean ratio of the simulated to the observed spectrum is not significantly different from unity at all frequencies (Figs. 4 and 5). The maximum excursion of the mean curve from unity in Figure 5 is a factor of 1.6 at approximately 10 Hz; at all other frequencies, it is less than a factor of 1.5. Inclusion of all, even more distant stations, narrows the confidence band on the mean (Figs. 4 and 5). There is no distinct dependence of standard deviation on whether the subset of 12 close stations (Fig. 4) or all rock stations (Fig. 5) are considered; at least, apart from irregular variations from frequency to frequency, no systematic trend is observed. The scatter of the ratio of the simulated to the observed spectrum, as characterized by one standard deviation, is between 0.3 and 2 at most frequencies, and it generally increases above 10 Hz. This gives the uncertainty in predicting individual spectra, which is also illustrated by the comparisons in Figure 3.

It is interesting to look at the cases where the simulations significantly underpredict site-specific observations (stations PKC, GPK, LPK, and ORR). We note that in each of them, the actual duration is significantly longer than the simulation. For example, at stations PKC and ORR, there are significant late-arriving low-frequency pulses in the observed traces, which are missing from the simulated records. However, at other stations near to PKC and ORR, the spectra and durations are well matched by the simulations. For example, at station PCD, only a few kilometers from PKC, the spectral amplitudes and duration of the simulation are a good match to the observations. At station ORR, the observed spectrum is underpredicted by almost an order of magnitude at low frequencies, while at nearby station L09, the observed spectrum is overpredicted at the same frequencies. It is possible that the significant discrepancies between the observations and the model at individual stations, such as ORR and PKC, are caused by the effects of local response, topography, or basin geometry unaccounted for by the simulations. Local response could be readily incorporated empirically and is likely to reduce the uncertainty of predictions at individual sites. Two-dimensional or three-dimensional basin effects are less easily incorporated, representing a limitation of the method. Overall, we conclude that the stochastic simulation provides a surprisingly accurate prediction of observed ground-motion amplitudes on average (Figs. 4 and 5), despite the simplicity of its underlying assumptions.

The hypocentral distance for stations used in this study varies by up to a factor of 4. Figure 6 presents the ratio of simulated to observed spectrum as a function of distance at example frequencies of 0.5 and 8 Hz, verifying that our adopted attenuation model is reasonable. There are no discernible distance-dependent trends in the model misfit.

In discussing the theoretical limitations of the method, we have suggested that simulations be confined to the frequency range where the subsource spectra are flat, or above the subsource corner frequency, to minimize the dependence

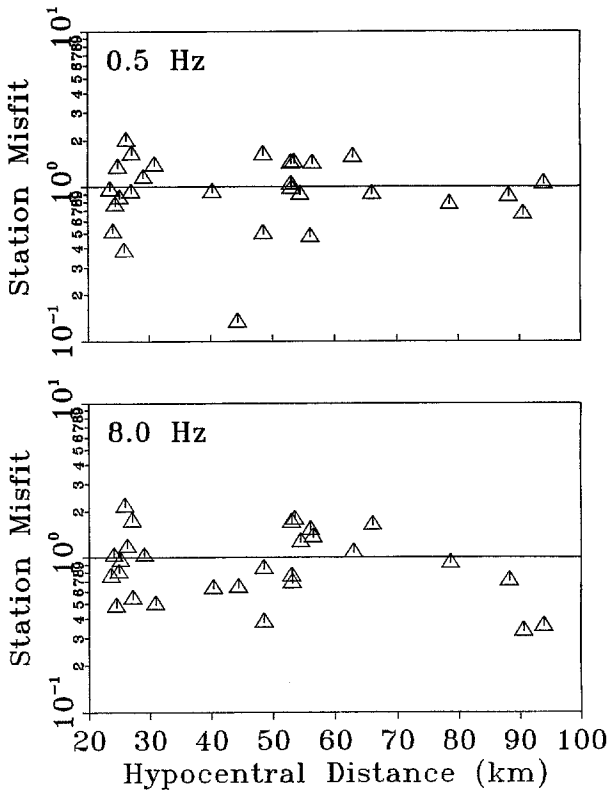

Figure 6. Station misfits (ratios of simulated to observed spectrum) as a function of hypocentral distance. Misfits are shown at 0.5 and 8 Hz.

of simulation results on the subfault size (Beresnev and Atkinson, 1998). The practical limits of applicability of the stochastic method, however, can only be established through empirical calibration. The corner frequency of the subsource spectra in Northridge simulations is 0.51 Hz. We performed simulations between 0.1 and 12.5 Hz and found no increase in modeling uncertainty toward the lowest frequencies. We thus suggest, based on the Northridge validation, that the application of the stochastic technique may be justified at frequencies as low as 0.1 Hz and higher.

It is interesting to check whether the slip velocity, derived from the calibrated value of the radiation-strength factor ($s = 1.6$), is consistent with other available estimates. Substituting the model parameters ($y = 0.8, z = 1.6 \times 1.68$, $\Delta\sigma = 50 \times 10^5$ N/m^2, $\rho = 2800$ kg/m^3, $\beta = 3700$ m/sec) into equation (3), we obtain $v_m = 0.8$ m/sec, which is the value implied by our simulations. The actual slip velocity may be estimated by dividing the average slip (1.3 m) by the average rise time (1.0 sec), provided by Wald *et al.* (1996, Table 5), to obtain $v_m = 1.3$ m/sec. The two values are in reasonable agreement, taking into account that each estimate has its uncertainty and is affected by a variety of model trade-offs.

Modeling with a Random Distribution of Slip

The simulation results discussed earlier have been obtained using the finite-fault model of Figure 2b, derived from Wald *et al.*'s (1996) distribution of slip for the mainshock rupture. In general, the distribution of slip is not known for future events. This motivates us to ask the question: How well could the ground motions be reproduced if the slip distribution or hypocenter location were not known? To answer this question, we repeat our simulations assuming a randomly drawn slip and hypocenter location. We assume that the geometry and location of a given seismogenic fault may be defined with reasonable accuracy, at least in principle; thus, we do not vary the location or geometry of the rupture surface.

We show the simulation results for two extreme cases of hypocenter location, corresponding to the upper left- and bottom right-hand corners of the fault (models A and B, respectively). The subfault moments are randomized in each case, with the constraint that the total moment be conserved. Due to the discrete character of the subevent moments, the resulting slip distribution could be more appropriately called quasi-random, since the subfault moments can only be multiples of m_0. The random finite-fault model A is shown in Figure 7, where the full 20- by 25-km fault area is assumed to have nonzero slip.

Figures 8 and 9 present the model bias and standard deviation for the random models A and B, estimated on the basis of the 12 close-in, and all 28 stations, respectively. As in the case of Figures 4 and 5, the use of data from all stations slightly narrows the confidence interval of the mean. Using the random slip models does not lead to any appreciable decrease in accuracy of predicting the mean nor does it increase the standard deviation, as compared to the actual slip derived from recorded geophysical data (cf. Figs 4 and 8, and 5 and 9). The mean ratio of simulated to observed spectrum remains indistinguishable from unity with 95% confidence. However, the misfit at individual stations will vary, due to directivity effects.

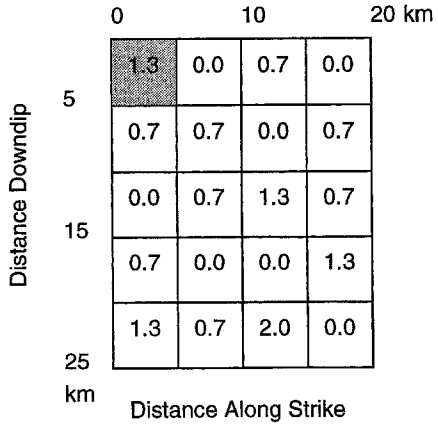

Figure 7 Finite-fault model with randomly drawn subevent moments. The numbers on subfaults indicate slip in meters. The hypocenter is at the center of the subfault shown in dark color.

Conclusions

The stochastic finite-fault radiation modeling technique (Beresnev and Atkinson, 1997, 1998) has been applied to simulating horizontal acceleration time histories for the 28 free-field rock recordings of the M 6.7 1994 Northridge, California, earthquake. The method provides an accurate prediction of the mean spectral content of ground motions: the ratio of the simulated to observed Fourier spectrum, averaged over all rock sites, is not significantly different from unity at the 95% confidence level, in the frequency range from 0.1 to 12.5 Hz.

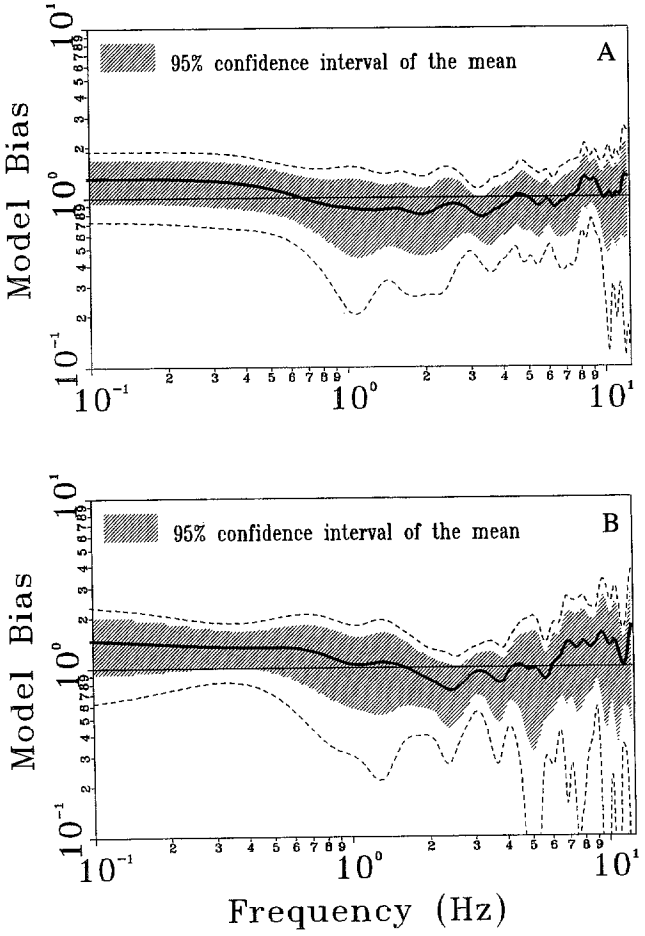

Figure 8. Model bias showing the ratio of simulated to observed spectrum, averaged over 12 close-in stations, for random-slip models A and B. Model A corresponds to the distribution of subevent moments and hypocenter location shown in Figure 7. Model B uses another random draw of the moment distribution, and the hypocenter is located at the bottom right-hand corner of fault plane. Dashed lines show ± 1 standard deviation.

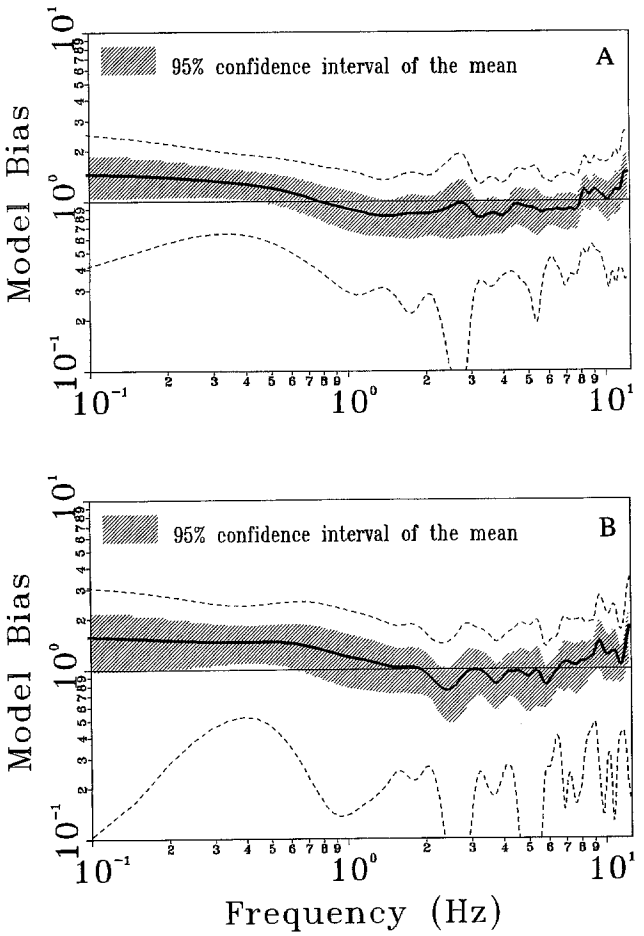

Figure 9. Model bias and standard deviation for all 28 stations, for random-slip models A and B.

We initially tested the method using the slip distribution derived from strong-motion, teleseismic, GPS, and leveling data (Wald *et al.,* 1996), most of which measure the low-frequency content of radiated energy. We subsequently tested the method using randomly generated moment distributions and two alternative hypocenter locations. The use of a randomly drawn slip model in place of the data-derived model does not lead to any appreciable increase in simulation uncertainty, on average. This suggests that knowledge of the slip distribution is not required for the accurate average prediction of acceleration spectra from large faults, for frequencies above 0.1 Hz. This conclusion is in accord with the general idea behind the stochastic method, which postulates that the character of ground acceleration is stochastic, reflecting complex source and path processes that are not readily modeled in deterministic terms (Hanks and McGuire, 1981).

Although our modeling suggests that the exact details of slip distribution or rupture initiation location are not necessary to match the mean observed acceleration spectra, the directivity effects strongly influence the peak ground accelerations (PGAs) at individual sites. This is clearly seen from the comparisons of PGA at stations situated directly updip and downdip of the fault plane, having similar hypocentral distance. Stations PCD and SSA are the most clear combination of this kind (Fig. 1 and Table 1). Both observed and predicted peak accelerations at station PCD are conspicuously higher than at station SSA (Fig. 3).

Also, although the model has a nearly zero average bias, the simulations of acceleration spectra at individual stations may have significant error. The model assumes a half-space geometry, which is shown to be correct on average. However, local response, surface topography, and basin effects can significantly affect the ground motions at individual sites. To generate more accurate ground-motion time histories at specific locations, empirical site-specific response functions would be useful.

Acknowledgments

Strong-motion data collected by the California Division of Mines and Geology, University of Southern California, United States Geological Survey, Southern California Earthquake Center, and Department of Energy were used in this study. We thank Alla and Alexei Tumarkin for helping us in access to the SCEC on-line data archive at the Institute of Crustal Studies, University of California, Santa Barbara. Figure 1 was produced with the Generic Mapping Tools (GMT) (Wessel and Smith, 1995). Special thanks go to D. Wald and the two anonymous reviewers whose suggestions helped to improve the manuscript. We are also grateful to Alexei Tumarkin for numerous discussions related to finite-fault modeling in the course of this work. This study was supported by the Natural Sciences and Engineering Research Council of Canada and by Grant 1434-HQ-97-GR-03061 of the National Earthquake Hazards Reduction Program. The FORTRAN code FINSIM used in the simulations with copies of all input files are available to all interested parties by writing to the authors.

References

Abrahamson, N. A., P. G. Somerville, and C. A. Cornell (1990). Uncertainty in numerical strong motion predictions, in *Proceedings of the Fourth U.S. National Conference on Earthquake Engineering,* Palm Springs, California, Vol. **1,** 407–416.

Anderson, J. and S. Hough (1984). A model for the shape of the Fourier amplitude spectrum of acceleration at high frequencies, *Bull. Seism. Soc. Am.* **74,** 1969–1993.

Atkinson, G. M. and I. A. Beresnev (1997). Don't call it stress drop, *Seism. Res. Lett.* **68,** 3–4.

Atkinson, G. M. and I. A. Beresnev (1998). Compatible ground-motion time histories for new national seismic hazard maps, *Canadian J. Civil Eng.* **25,** 305–318.

Atkinson, G. M. and D. M. Boore (1997). Stochastic point-source modeling of ground motions in the Cascadia region, *Seism. Res. Lett.* **68,** 74–85.

Atkinson, G. M. and D. M. Boore (1998). Evaluation of models for earthquake source spectra in eastern North America, *Bull. Seism. Soc. Am.* **88,** 917–934.

Atkinson, G. M. and W. Silva (1997). An empirical study of earthquake source spectra for California earthquakes, *Bull. Seism. Soc. Am.* **87,** 97–113.

Beresnev, I. A. and G. M. Atkinson (1997). Modeling finite-fault radiation from the ω^n spectrum, *Bull. Seism. Soc. Am.* **87,** 67–84.

Beresnev, I. A. and G. M. Atkinson (1998). FINSIM —a FORTRAN program for simulating stochastic acceleration time histories from finite faults, *Seism. Res. Lett.* **69,** 27–32.

Beresnev, I. A., G. M. Atkinson, P. A. Johnson, and E. H. Field (1998). Stochastic finite-fault modeling of ground motions from the 1994 Northridge, California, earthquake. II. Widespread nonlinear response at soil sites, *Bull. Seism. Soc. Am.* **88,** 1402–1410.

Boore, D. M. (1983). Stochastic simulation of high-frequency ground motions based on seismological models of the radiated spectra, *Bull. Seism. Soc. Am.* **73,** 1865–1894.

Boore, D. M. (1986). Short-period *P*- and *S*-wave radiation from large earthquakes: implications for spectral scaling relations, *Bull. Seism. Soc. Am.* **76,** 43–64.

Boore, D. M. (1996). SMSIM—Fortran programs for simulating ground motions from earthquakes: version 1.0, *U.S. Geol. Surv. Open-File Rept. 96-80-A,* 73 pp.

Boore, D. and G. Atkinson (1987). Stochastic prediction of ground motion and spectral response parameters at hard-rock sites in eastern North America, *Bull. Seism. Soc. Am.* **77,** 440–467.

Boore, D. M and W. B. Joyner (1997). Site amplifications for generic rock sites, *Bull. Seism. Soc. Am.* **87,** 327–341.

Chang, S. W., J. D. Bray, and R. B. Seed (1996). Engineering implications of ground motions from the Northridge earthquake, *Bull. Seism. Soc. Am.* **86,** S270–S288.

Chin, B.-H. and K. Aki (1991). Simultaneous study of the source, path, and site effects on strong ground motion during the 1989 Loma Prieta earthquake: a preliminary result on pervasive nonlinear site effects, *Bull. Seism. Soc. Am.* **81,** 1859–1884.

Hanks, T. C. and R. K. McGuire (1981). The character of high frequency strong ground motion, *Bull. Seism. Soc. Am.* **71,** 2071–2095.

Hartzell, S. H. (1978). Earthquake aftershocks as Green's functions, *Geophys. Res. Lett.* **5,** 1–4.

Hartzell, S., A. Leeds, A. Frankel, and J. Michael (1996). Site response for urban Los Angeles using aftershocks of the Northridge earthquake, *Bull. Seism. Soc. Am.* **86,** S168–S192.

Heaton, T. H. and S. H. Hartzell (1989). Estimation of strong ground motions from hypothetical earthquakes on the Cascadia subduction zone, Pacific Northwest, *Pure Appl. Geophys. (Pageoph)* **129,** 131–201.

Hutchings, L. (1994). Kinematic earthquake models and synthesized ground motion using empirical Green's functions, *Bull. Seism. Soc. Am.* **84,** 1028–1050.

Irikura, K. (1983). Semi-empirical estimation of strong ground motions during large earthquakes, *Bull. Disaster Prevention Res. Inst. Kyoto Univ.* **33,** 63–104.

Joyner, W. B. and D. M. Boore (1986). On simulating large earthquakes by Green's-function addition of smaller earthquakes, in *Proceedings of the Fifth Maurice Ewing Symposium on Earthquake Source Mechanics,* S. Das, J. Boatwright, and C. Scholz (Editors), American Geophysical Union, 269–274.

Kanamori, H. and D. L. Anderson (1975). Theoretical basis of some empirical relations in seismology, *Bull. Seism. Soc. Am.* **65,** 1073–1095.

Schneider, J. F., W. J. Silva, and C. Stark (1993). Ground motion model for the 1989 *M* 6.9 Loma Prieta earthquake including effects of source, path, and site, *Earthquake Spectra* **9,** 251–287.

Silva, W. J., R. Darragh, and I. G. Wong (1990). Engineering characterization of earthquake strong ground motions with applications to the Pacific Northwest, in *Proceedings of the Third NEHRP Workshop on Earthquake Hazards in the Puget Sound/Portland Region,* W. Hays (Editor), *U.S. Geol. Surv. Open-File Rept.*

Somerville, P., M. Sen, and B. Cohee (1991). Simulations of strong ground motions recorded during the 1985 Michoacán, Mexico and Valparaíso, Chile, earthquakes, *Bull. Seism. Soc. Am.* **81,** 1–27.

Toro, G. R., N. A. Abrahamson, and J. F. Schneider (1997). Model of strong ground motions from earthquakes in central and eastern North America: best estimates and uncertainties, *Seism. Res. Lett.* **68,** 41–57.

Tumarkin, A. G. and R. J. Archuleta (1994). Empirical ground motion prediction, *Ann. Geofis.* **37,** 1691–1720.

Tumarkin, A. G., R. J. Archuleta, and R. Madariaga (1994). Scaling relations for composite earthquake models, *Bull. Seism. Soc. Am.* **84,** 1279–1283.

Tumarkin, A. A., A. G. Tumarkin, and R. J. Archuleta (1996). SMDB: strong-motion database. User's guide, Institute for Crustal Studies, University of California, Santa Barbara.

Wald, D. (1997). Surfing the Internet for strong-motion data, *Seism. Res. Lett.* **68,** 766–769.

Wald, D. J., T. H. Heaton, and K. W. Hudnut (1996). The slip history of the 1994 Northridge, California, earthquake determined from strong-motion, teleseismic, GPS, and leveling data, *Bull. Seism. Soc. Am.* **86,** S49–S70.

Wessel, P. and W. H. F. Smith (1995). New version of the Generic Mapping Tools released, *EOS* **76,** 329.

Zeng, Y., J. G. Anderson, and G. Yu (1994). A composite source model for computing realistic strong ground motions, *Geophys. Res. Lett.* **21,** 725–728.

Department of Geological & Atmospheric Sciences
Iowa State University
253 Science I
Ames, Iowa 50011-3212
E-mail: beresnev@iastate.edu
(I.A.B.)

Department of Earth Sciences
Carleton University
1125 Colonel By Drive
Ottawa, Ontario K1S 5B6, Canada
E-mail: gma@ccs.carleton.ca
(G.M.A.)

Manuscript received 13 January 1998.